Dyes and Pigments 116 (2015) 27–35

Contents lists available at ScienceDirect

Dyes and Pigments

journal homepage: www.elsevier.com/locate/dyepig

New azine compounds as photoantimicrobial agents against *Staphylococcus aureus*

María N. Urrutia [a], Fabiana L. Alovero [a, b], Cristina S. Ortiz [a, *]

[a] Departamento de Farmacia, Facultad de Ciencias Químicas, Universidad Nacional de Córdoba, Ciudad Universitaria, X5000HUA Córdoba, Argentina
[b] UNITEFA-CONICET, Argentina

ARTICLE INFO

Article history:
Received 24 September 2014
Received in revised form
19 December 2014
Accepted 23 December 2014
Available online 31 December 2014

Keywords:
Neutral Red
Monobrominated Neutral Red
Staphylococcus aureus
Singlet oxygen
Aggregation
Lipophilicity

ABSTRACT

Aggregation phenomena of Neutral Red and a new derivative monobrominated Neutral Red were examined in different buffer solutions as a function of dye concentration. The dyes were chemically and photochemically stable and the lipophilicity of the new bromo-compound was characterized by experimental and computer prediction data. In addition, the acid dissociation constant and the singlet molecular oxygen production were determined spectrophotometrically yielding values of 1.16 and 3.14 for Neutral Red and the monobrominated derivative, respectively.

The effect of photosensitizer concentration, visible irradiation time and cellular density on lethal photosensitization against *Staphylococcus aureus* were investigated. The improved physicochemical and photophysical properties of monobrominated Neutral Red were accompanied by a significant increase in the photoantimicrobial action, in conventional-sensitive and -resistant isolates.

Based on these results, the dyes exhibited favorable properties; therefore, the new derivative compound could be a promising sensitizer with applications in the photoinactivation of *S. aureus*.

1. Introduction

Photodynamic Therapy (PDT) and Photodynamic Antimicrobial Chemotherapy (PACT) are technologies that utilize visible light, oxygen and photosensitizers (PS) to inactivate cells [1,2].

PDT represents a well-established therapeutic modality, which was originally developed and approved for the treatment of a variety of solid tumors [3]. The increase in the development of antimicrobial resistance demands the search of alternative treatment strategies. PACT emerged as a new treatment modality for microbial infections because of its efficiency and lower potential for resistance development [4,5]. The photoactivation of a PS at the action site with light of specific wavelength, results in the destruction of cells by a complex cascade of chemical, biological and physiological reactions that occur after the formation of highly reactive oxygen species such as singlet oxygen [6,7].

An ideal PS should be a single and pure compound with a stable composition, selective to the target cells; it should be non-toxic, should have high singlet oxygen quantum yield and should not form aggregates in solution [8].

Neutral Red (NR) is a phenazine-based dye with many applications in biology, and has been used for various purposes in cytometry such as a probe in model biological systems, an intracellular pH indicator (pH sensor) in the pH range 6–8 and a specific lysosomal probe because of its weak base properties [9–11]. Now it finds application as a probe for neuronal activity [11]. NR is a good PS in phototherapy and has been reported to interact with several substrates in a type I reaction [11,12]. This dye has been tested against Herpes Simplex Virus Type 1 which was inactivated after irradiation by light at a wavelength of 470 nm [13]. Currently, little is known about the potential effectiveness of NR as PS against bacterial species of interest in the clinical setting. Without detailed studies of its efficacy as PS [14], only minimum lethal concentration values of NR have been reported in literature so far.

In our earlier work [15], the synthesis of a new compound, monobrominated Neutral Red (NRBr) was described. Due to the introduction of a heavy atom into the molecule, the efficiency of a spin-forbidden electronic transition from a singlet to a triplet state (intersystem crossing) is increased leading to a greater quantity of singlet oxygen ($^1O_2$) [16,17]. This newly synthesized phenazine dye has demonstrated potential use as a PS because it presents less aggregation in different solvents in comparison with the parent

* Corresponding author. Tel.: +54 351 5353865x53356; fax: +54 351 5353865x53364.
E-mail address: crisar@fcq.unc.edu.ar (C.S. Ortiz).

http://dx.doi.org/10.1016/j.dyepig.2014.12.021
0143-7208/

compound. The chemical structures of NR and NRBr are shown in Scheme 1.

Since aggregation modifies the absorption spectrum and the photophysical and photochemical properties of a dye and affects its ability to act as a PS [18,19], the influence of NRBr concentration in different buffer solutions on the aggregate formation was examined, and these results were then compared with NR dye in identical experimental conditions.

Additionally, the acid–base dissociation constant (pK_a), the stability, photostability and octanol–water partition coefficient were evaluated [20–25]. Also, a comparison between the experimental log P_{HPLC} and the calculated values using different computer programs was included. The capacity of NR and NRBr to produce singlet oxygen ($^1O_2$), was determined as well [26,27].

Finally, the photoantimicrobial effect was explored and, in this context, the efficiency of PACT exhibited by NR and NRBr against *Staphylococcus aureus* was determined in a comparative study that evaluated both sensitive- and resistant-isolates to currently-used antimicrobial agents.

2. Experimental section

2.1. General

2.1.1. Materials/chemicals

Neutral Red hydrochloride (3 amino-7-dimethylamino-2-methyl phenazine hydrochloride) was purchased from Sigma Chemical Co. (St. Louis, MO) (Fluka Chemicals) and its purity was confirmed by RP-HPLC (>98%). Monobrominated Neutral Red was synthesized in our laboratory according to the procedure previously described [15].

Buffer solutions were prepared from hydrochloric acid (37%)/potassium chloride (pH 1.2), hydrochloric acid (37%)/potassium hydrogen phthalate (pH 2.5 and 4.0), potassium dihydrophosphate/sodium hydroxide (pH 5.8, 6.2, 6.7 and 7.4), hydrochloric acid (37%)/sodium borate (pH 9.0) and sodium hydroxide/sodium bicarbonate (pH 11.0). The ionic strength of the buffer solutions was adjusted to 0.5 M using sodium chloride (Cicarelli) as a supporting electrolyte and the pH was determined by a CRISON GLP 21 pH-meter using a combined glass electrode. Phosphate-buffered saline (PBS, 10 mM pH 7.4) solution was prepared using sodium chloride, potassium chloride, sodium hydrogen phosphate dihydrate and potassium dihydrophosphate. All the high purity grade chemicals were obtained commercially (Cicarelli, Anedra) and the solutions were prepared using ultrapure water from Milli-Q® purification system (Millipore Corporation, USA). All the solvents used were of pro-analysis or HPLC grade quality (Cicarelli, Sintorgan, Anedra).

2.1.2. Instrumentation

Absorption spectra were carried out at room temperature with an Evolution 300 spectrophotometer between 200 and 700 nm, using 1 cm path length quartz cells. Stock solutions of dyes were freshly made in duplicate and then diluted appropriately with the same media. All experiments were carried out at least twice with consistent results.

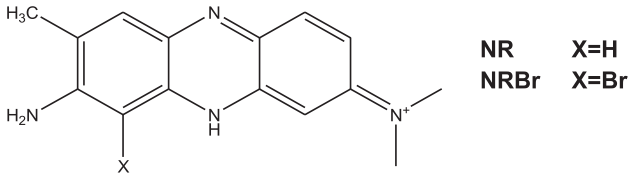

Scheme 1. Molecular structure of Azine dyes.

The RP-HPLC measurements were performed on an Agilent Series 1100 chromatograph (Agilent Technologies, Waldbronn, Germany) equipped with an autosampler, a column thermostat, an UV–vis detector and a reversed-phase C18 Phenomenex® column (4.6 mm × 250 mm, 5 μm) with a guard column. The column temperature was set at 25 °C and the flow rate at 1.0 mL/min. The mobile phases and the samples prepared in the mobile phases were filtered through a Millipore® Type FH filter (0.45 μm pore size). Subsequently, the mobile phases were vacuum degassed. Data were produced by means of a Peak Simple Chromatography Data System®.

The chemical stability of the dyes was evaluated using a thermostatic bath Vicking® Masson D. In the illuminated experiences, samples were irradiated at 5 cm of distance with a Parathom® lamp (OSRAM – 5 W). The fluence rate measured with a Tes 1332 Digital Lux Meter (TES Electrical Electronic Corp.) was 8.4 mW/cm^2.

2.2. Evaluation of azine photosensitizers

2.2.1. pK_a determination and aggregation behavior in different buffer solutions

Spectral curves for pK_a determination were recorded in different buffer solutions (pH range 1.2–11.0) at 1.39×10^{-5} M and 2.71×10^{-5} M for NR and NRBr respectively, because the absorbances of the cationic and nonionic species were in the range of the lowest spectrophotometric error. The pK_a of the dyes was determined from the second-derivative of absorbance (at the λ_{max} of the cationic species) against the pH of the solution. Aggregation of NR and NRBr as a function of dye concentration (10^{-6} M to 10^{-4} M) was studied by means of the spectral curves in buffer solutions at pH 1.2, 5.8 and 7.4.

2.2.2. Stability and photostability tests

The chemical stability of the dyes was evaluated in buffer solutions at pH 1.2, 5.8 and 7.4 at 37 °C by UV–visible spectroscopy and the samples were protected from the light. For all the experiments the concentration of the dyes was 10^{-5} M and the samples were withdrawn at 1 h intervals for 32 h.

The photostability of the dyes (10^{-5} M) in buffer solution (pH 7.4) at room temperature was carried out in quartz cells that were irradiated (Experimental Section: 2.1.2 Instrumentation) for 120 min (total light dose 60.5 J/cm^2). The solutions of the dyes were monitored by UV–visible spectroscopy as a function of time.

Parameters such as selectivity, linearity, accuracy, precision, limit of detection (LOD) and limit of quantitation (LOQ) for the stability and photostability studies were also determined (data not shown).

The absence of degradation products was corroborated by RP-HPLC using methanol: aqueous solution of trimethylammonium phosphate 83 mM (70:30 v/v) as mobile-phase.

2.2.3. Determination of log P

2.2.3.1. Log P_{HPLC}. The HPLC general procedure consisted of measurement of the retention time under isocratic conditions with varying amounts of methanol as an organic modifier (φ) since it is the best solvent for the chromatographic determinations [28].

Methanol-buffer pH 7.4 mixtures, with methanol content between 65% and 90% (v/v) in 5% increments (final pH from 8.9 to 9.5) were used as mobile phases. The buffer pH 7.4 (10 mM) was prepared with potassium phosphate monobasic (19.7%) and sodium phosphate dibasic (80.3%) in Milli-Q® water.

A multiwavelength UV–visible detector was fixed at 280 nm and at the λ_{max} of the reference compounds and NRBr (Table 1), which were injected in triplicate. Seven structurally related compounds were evaluated as references in order to establish the log $P_{O/W}$ – log k_w relationship. Their partition coefficient (log $P_{O/W}$) values covering a wide range of lipophilicity were taken from the literature (2.83–6.58) (Table 1).

Table 1
Determination of Log P_{HPLC} values.

Compounds	λ_{max} (nm)	Log $P_{O/W}$[a]	φ	S	Log k_w[b]	r	Log P_{HPLC}
References							
Cresyl Violet	590	2.83	65–85	−0.031 ± 0.002	2.3 ± 0.1	0.98734	2.9 ± 0.1
Neutral Red (NR)	540	3.20	65–85	−0.033 ± 0.002	2.6 ± 0.1	0.99066	3.2 ± 0.1
Phenanthrene	280	4.52	70–90	−0.044 ± 0.005	4.2 ± 0.4	0.95620	4.5 ± 0.4
Anthracene	250	4.56	70–90	−0.046 ± 0.003	4.4 ± 0.2	0.98614	4.7 ± 0.2
Crystal Violet	590	4.95	65–85	−0.060 ± 0.005	4.8 ± 0.2	0.97428	5.0 ± 0.2
9-bromo-phenanthrene	280	5.45	70–90	−0.052 ± 0.004	5.1 ± 0.3	0.97879	5.3 ± 0.3
Rose Bengal	550	6.58	65–90	−0.083 ± 0.003	6.8 ± 0.2	0.99362	6.7 ± 0.3
Test substance							
Neutral Red monobrominated (NRBr)	540	–	65–85	−0.039 ± 0.002	3.3 ± 0.1	0.99293	3.8 ± 0.1

[a] Literature data.
[b] n = 3.

The capacity factor (k') of all compounds were calculated from the experimentally determined retention data using eq. (1)

$$k' = (t_R - t_0)/t_0 \quad (1)$$

where t_R is the retention time of the solute and t_0 is the dead time that is defined as the retention time of a non-retained compound which was determined by injection of methanol [28].

The log k' values for each reference compound and the substance tested were plotted against the volume percent of methanol in the eluent (φ) based on the established linear relationship (eq. (2)), where S is the slope.

$$\log k' = S \cdot \varphi + \log k_w \quad (2)$$

The log k' values for each compound (log k_w) corresponding to 100% aqueous solution (0% modifier) were obtained by extrapolation. In this case, as k' is independent of the organic modifier effect, the polar–non-polar partitioning will be more similar to the shake measurements and dependent on the solute structure and polar functionalities [29].

A plot of log k_w versus log $P_{O/W}$ (eq. (3)) was generated for the reference compounds:

$$\log P_{O/W} = \boldsymbol{a} \log k_w - \boldsymbol{b} \quad (3)$$

In the next step, coefficients ***a*** and ***b*** were obtained and the log k_w value of NRBr was used to calculate its partition coefficient (log P_{HPLC}) using the eq. (4),

$$\log P_{HPLC} = \boldsymbol{a} \log k_w - \boldsymbol{b} \quad (4)$$

Regression and correlation analyses were performed with OriginPro 8 SR0 (OriginLab Corporation).

2.2.3.2. Theoretical calculation of log P (clog P). Different types of software allowing theoretical calculations of various lipophilicity descriptors, on the basis of obtained geometry of the molecule [30] were used. For purposes of comparison, the theoretical partition coefficients (clog P) of the compounds were calculated by a fragment-based approach employing commercially available chemical software ACD/logP program Version 6.0 (Toronto, Canada) and programs available as a freeware: Molinspiration Cheminformatics Software (miLogP 2.2) and OSIRIS Property Explorer.

Correlation between the experimental data (log k_w) and the software that predicted lipophilicity (clog P) was compared by linear regression analysis (eq. (5)) determining the parameters of the relationship.

$$\text{clog P} = a \log k_w + b \quad (5)$$

2.2.4. Photodynamic properties: singlet oxygen determination

Solutions of NR and NRBr dyes were irradiated (Experimental Section: 2.1.2 Instrumentation) in quartz cells of 1 cm path length with 9,10-dimethylanthracene (DMA, absorbance ~0.6) in *N,N*-dimethylformamide (DMF). To ensure that in all experiments an equal number of photons were absorbed per unit time, the concentration for each dye was adjusted at an absorbance of ~0.18 at the λ_{max}. The kinetics of DMA photooxidation were studied by following the decrease of the absorbance (A) at $\lambda_{max} = 378$ nm as a function of irradiation time. The observed rate constants (k_{obs}) were obtained by a linear least-squares fit of the semilogarithmic plot of Ln (A_0/A) versus time, and the values of singlet oxygen quantum yields (Φ_Δ) relative to methylene blue dye used as reference (MB, $\Phi_\Delta = 1$) were calculated.

The Φ_Δ of the NR and NRBr was calculated using eq. (6), where PS is the photosensitizer, Ref is the reference compound and A is the initial absorbance at 378 nm.

$$\Phi_\Delta^{PS} = \frac{\Phi_\Delta^{Ref}\, k_{obs}^{PS}\, A^{Ref}}{k_{obs}^{Ref}\, A^{PS}} \quad (6)$$

2.2.5. PACT studies

2.2.5.1. Bacterial cultures. The bacteria used in this study were *S. aureus* ATCC 25923 and a clinical isolate of *S. aureus* resistant to methicillin and fluoroquinolones (MRSA61). Organisms were maintained by weekly subculture on Müeller-Hinton agar (Britania, Buenos Aires, Argentina). An overnight culture was suspended in PBS and adjusted to a bacterial concentration of ~ 5×10^7 CFU/mL (corresponding to 0.5 Mc Farland scale). In some experiments, cells were diluted in PBS, corresponding to ~ 5×10^5 CFU/mL, to compare cellular density effect.

2.2.5.2. Photodynamic inactivation of bacteria in vitro. Effect of PS concentration (range 5–200 μM), irradiation time (15, 30, 60 min, total light dose 7.6; 15.1 and 30.2 J/cm^2, respectively) (Experimental Section: 2.1.2 Instrumentation) and cellular density (10^5 and 10^7 CFU/mL) on lethal photosensitization were investigated.

In all the experiments, 1 mL of the cell suspensions in culture tubes (13 × 100 mm) was used and 1 mL of the sensitizer was added. Cultures were exposed to visible light at different time intervals.

Bacterial cultures grown under the same conditions with and without PS kept in the dark as well as illuminated cultures without sensitizer served as controls.

At the completion of the illumination period, 100 μL aliquots were removed from illuminated and non-illuminated tubes and

serially diluted 10-fold into PBS to give concentrations of 10^{-1}–10^{-5} times of the original concentrations. Viable bacteria were monitored by subculturing 100 μL of the appropriated dilution on Müeller-Hinton agar plates in duplicate. Then, the number of colonies formed after 18–24 h incubation at 37 °C was counted. Data (CFU/mL) were log-transformed and both PS were compared with the control cultures.

Each time-dependent killing experiment was performed on three independent occasions and the data were expressed as the average of all values obtained.

Statistics values were expressed as the mean ± standard deviation of each group. The difference between two means was compared by a two-tailed unpaired Student's *t* test. P values of <0.05 were considered significant.

3. Results and discussion

3.1. pK_a determination

The spectra of NRBr are strongly pH dependent, exhibiting the cationic form of dye at pH 1.2, 2.5 and 4.0 with λ_{max} approximately at 530 nm. On the other hand, buffer solutions of NRBr at pH 7.4 are colorless since the nucleophile OH^- ion abstracts the H^+ from the cationic form generating nonionic aromatic species because the central nitrogen atom of the dye is electron-deficient [11] (See 3.3 Stability and Photostability tests).

The spectra of NRBr at pH 5.8, 6.2 and 6.8 presented two bands at $\lambda = 530$ nm and at approximately $\lambda = 470$ nm, which was attributed to the higher order aggregates (See 3.2 Aggregation behavior in different buffer solutions). The band at 470 nm is not assigned to the neutral species of the dye because it disappears in solutions of pH higher than 6.8. However, the NR solutions keep the color at high pH values because the NR solutions turn yellow and the NRBr ones colorless at higher pH than that of their pK_a.

An interesting observation was made when a drop of chlorhydric acid was added to the yellow or colorless solutions of NR and NRBr, which immediately turned red and violet respectively. This indicates that the acidic medium destabilizes the benzenoid forms and regenerates the ionic species, and suggests that the dye–OH interaction/H abstraction are weak and reversible. Conversely, these quinonoid forms (ionic species) of both compounds, upon alkaline solution, regenerate the nonionic species because OH^- abstracts H^+ and makes the molecule fully aromatic [11].

The pK_a value of NRBr was determined from the second derivative of the absorbance of the dye versus the pH of the buffer solutions (pK_a NRBr = 5.8 ± 0.1). Besides, the pK_a of NR was determined (pK_a NR = 7.0 ± 0.8) following the same procedure to corroborate the value previously reported in the literature [31,32]. Fig. 1 shows the absorbance versus the pH of the solution and the second derivative of the absorbance of NRBr dye at the λ_{max} of the cationic species versus the pH of the solution.

The pK_a values obtained for both compounds indicate that these chromophores undergo a protonation/deprotonation reaction. This demonstrates that the nonionic benzenoid species are acid sensible. Halogenation significantly lowers the pK_a value of the dye in accordance with the electron withdrawing character of the halogen atoms [27]. This lowering of pK_a could be beneficial because the NRBr would be present in the biological system as a mixture of neutral and cationic forms. This fact could allow the dye to be incorporated and accumulated into cells whose lower pH could facilitate the dye protonation. A marked change in the absorption spectrum is associated with the deprotonation process which should be considered during cell photoradiation investigations. This is particularly relevant for the dyes investigated in this study because both have pK_a values close to the physiological pH [27].

3.2. Aggregation behavior in different buffer solutions

In order to analyze NR and NRBr aggregation behavior, the absorption spectra in physiological pH conditions (pH 1.2, 5.8 and 7.4) were studied and compared.

In our earlier work, the monomeric species of NR and NRBr in different organic solvents at approximately λ_{max} 450 nm were reported. For both dyes in aqueous solution, an absorption band, assigned to the aggregated form of dyes [15], was determined at approximately λ_{max} 535 nm.

Accordingly, the absorption spectra of the protonated form of NR in buffer solution pH 1.2 at different dye concentrations (from 1.39×10^{-6} M to 9.70×10^{-5} M) showed a blue shift of maximum absorption wavelength (H-band) from λ_{max} 532 nm to λ_{max} 523 nm when the dye concentration increased (S1 Supporting information). Besides, an isosbestic point was observed at 587 nm and the Lambert–Beer law was found to be non-linear. The band at 530 nm was assigned to the aggregated form of NR and the blue shift observed as a function of the dye concentration in that buffer solution, was attributed to the higher order aggregates (S1 inset Supporting information). The monomeric species of this dye could not be seen at pH 1.2, but a similar blue shift was observed in the pH 5.8 buffer solution.

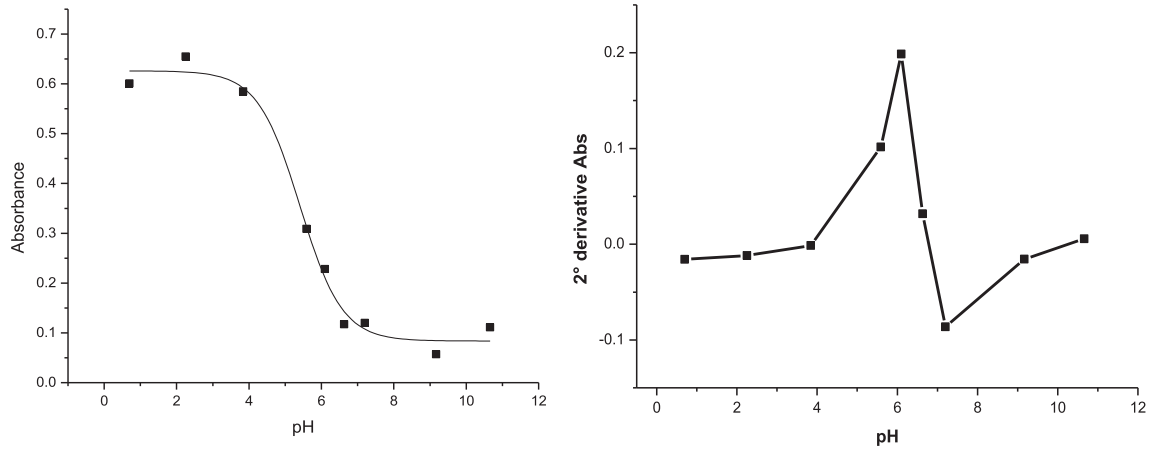

Fig. 1. (Right) Absorbance at the λ_{max} of the cationic species of NRBr dye versus pH of the solution. (Left) Second-derivative of the absorbance of the NRBr versus pH of the solution.

As shown in Fig. 2, the absorption spectra of NR at pH 7.4 suggest the deprotonation of the cationic species because these spectra exhibited two absorption bands: a maximum at 528 nm, which belongs to the cationic form of the aggregated dye, and a shoulder at approximately 470 nm corresponding to the neutral form of NR [31–33]. The band attributed to the aggregated cationic form of the NR presented an isosbestic point at 572 nm and a blue-shift of 16 nm (λ_{max} from 528 nm to 512 nm) as a function of dye concentration.

Conversely, it is evident from the normalized absorption spectra (Fig. 2) that the band assigned to the aggregated neutral species of NR (at approximately 470 nm) showed an increase in the absorption as a function of dye concentration, in comparison with the cationic form. This increase was attributed to the formation of the higher order aggregates of the neutral species. For the first time, we report the presence of the cationic and neutral forms of the NR dye at pH 7.4 at concentrations ranging from 6.93×10^{-6} M to 7.62×10^{-5} M.

The new NRBr dye was evaluated at pH = 1.2 and at different concentrations (1.08×10^{-6} M to 9.49×10^{-5} M) (data not shown). The absorption spectra of NRBr presented, at the lowest dye concentration, a λ_{max} = 541 nm and, at the highest concentration, a λ_{max} = 529 nm. Because of the increase in the NRBr concentration, a blue shift of 12 nm and an isosbestic point at about 600 nm were observed. This displacement can be explained in the same terms as for the NR dye.

The normalized absorption spectra of NRBr at pH 5.8 recorded at different dye concentrations are shown in Fig. 3. At lower dye concentrations (<1.39×10^{-4} M), NRBr exhibited a maximum absorption at 537 nm and a shoulder at about 468 nm. At higher concentrations, this 468 band became the maximum of the spectral curve. The band at 537 nm was attributed to the aggregated form of NRBr, while the new spectral maximum observed at 468 nm was assigned to the higher order aggregates. These changes were marked by the presence of an isosbestic point at 580 nm, suggesting the formation of the aggregated species.

The absorption spectra of NRBr in ultrapure Milli-Q® water (pH 5.76) have been previously discussed [15]. At lower concentrations of dye, an absorption band at 468 nm was observed and attributed to the monomer form of NRBr. The shoulder at 535 nm became the new spectral maximum with an increase in the dye concentration, which was attributed to the aggregated form.

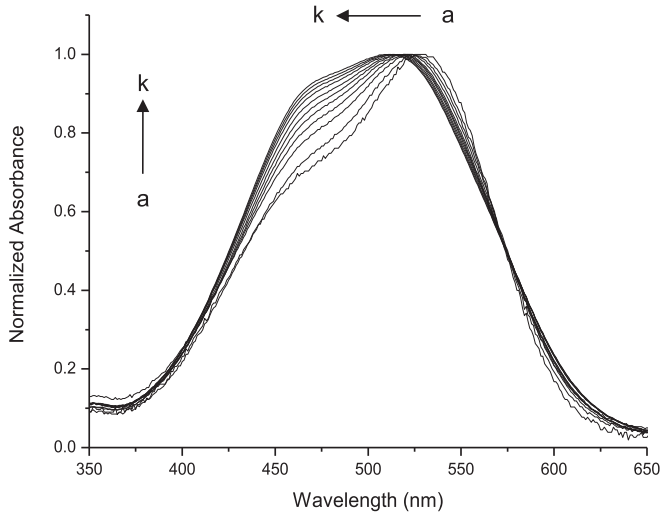

Fig. 2. Normalized absorption spectra of NR in buffer pH = 7.4 at maximum absorption wavelength as a function of dye concentration. [NR] (a) 6.93×10^{-6} M, (k) 7.62×10^{-5} M.

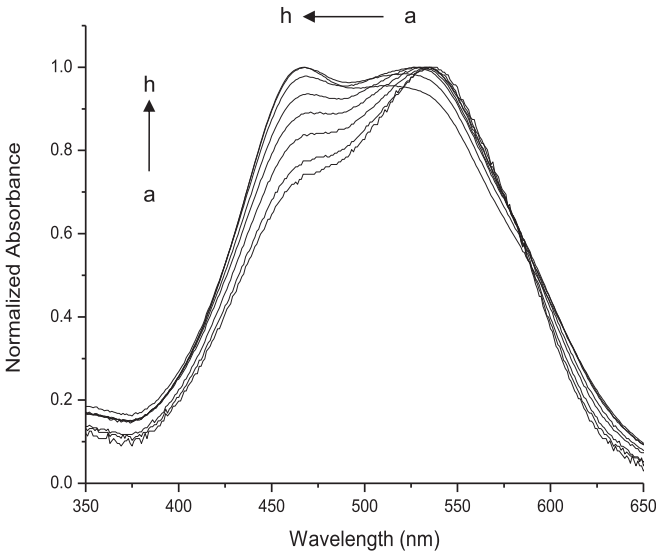

Fig. 3. Normalized absorption spectra of NRBr in buffer pH = 5.8 at maximum absorption wavelength as a function of dye concentration. [NRBr] (a) 3.25×10^{-5} M, (h) 2.71×10^{-4} M.

The comparison of the NRBr spectra in buffer solution at pH 5.8 (Fig. 3) and in Milli-Q® water indicated that the difference observed between them could be explained by the high ionic strength of buffer at pH 5.8 (0.5 M) which increases the aggregation effect; therefore, higher order aggregates could be seen in this buffer solution, according to the literature [18,34]. Besides, in buffer solution at pH 7.4, the neutral form of the NRBr is colorless, so the spectral curves could not be discussed.

3.3. Stability and photostability tests

The results obtained for NR and NRBr demonstrated a high chemical stability in the buffer solutions assayed at 37 °C during 32 h (data not shown). The NRBr dye in buffer solutions at pH 5.8 and 7.4 was gradually decolorized as a function of time; however, this effect was almost completely reversed by the addition of hydrochloric acid to the solutions previously analyzed by UV–vis spectroscopy, indicating an equilibrium between cationic form and nonionic species. (See 3.1 pK_a determination).

This dye was studied in Milli-Q® water (pH 5.76) to evaluate if the composition of the buffer solutions was involved in the NRBr discoloration process. After the experiment, a similar discoloration of the solution was observed, so the buffer composition is not involved in this effect.

According to these results, the NRBr discoloration at pH 5.8 and 7.4 is due to the presence of neutral species of the dye, which showed its typical acid-based equilibrium.

On the other hand, NR and NRBr presented high photostability during 120 min of irradiation (data not shown), which was evidenced by the overlapping of the spectral curves as a function of time and the absence of the degradation products analyzed by RP-HPLC.

3.4. Determination of log P

3.4.1. Log P_{HPLC}

Correlation between the log k' values and the composition of the mobile phase (φ between 65% and 90%) for the reference compounds (eq. (2)) showed a linear relationship (Table 1). It is possible to note that the slope is always negative when it is related to the

hydrophobic surface of the molecule which interacts with the non-polar stationary phase [28]. The log k_w values for all compounds were calculated and the correlation between these data and log $P_{O/W}$ for the reference compounds was expressed by eq. (7) with excellent fit.

$$\log P_{O/W} = (0.84 \pm 0.03) \log k_w + (1.0 \pm 0.1) \quad (7)$$

$n = 7$; $r = 0.99576$; $r^2 = 0.99154$; $s = 9.86457$; $F = 704.35$

For all compounds, log P_{HPLC} was calculated according to the eq. (8). The values are shown in Table 1.

$$\log P_{HPLC} = (0.84 \pm 0.03) \log k_w + (1.0 \pm 0.1) \quad (8)$$

Lipophilicity for solutes increased due to electron-withdrawing bromine-substituents, as can be seen when log P_{HPLC} obtained for NR and NRBr was compared.

The penetration of PS molecules into the cell depends on their size, charge, solubility and also on the cell type. They may accumulate at particular subcellular locations or be associated with the most hydrophobic regions of membranous organelles [26]. The lipophilic parameter of a drug candidate seems to be the most important physicochemical parameter in the structure–activity relationship studies [35] because it showed that an increase in lipophilicity leads to a higher cellular uptake which is usually correlated with an increased biological activity [36].

3.4.2. Theoretical calculation of log P (clog P)

Comparison between the experimentally measured log k_w and computer estimated lipophilicity parameters revealed a good linear correlation for the set of evaluated compounds (eq. (5)). Parameters and statistical data of correlation between log k_w and clog P values are shown in Table 2.

The highest correlation obtained by OSIRIS program was satisfactory. Two good linear correlations were also obtained using miLogP and ACD/logP. The three correlations showed "r" values from 0.913 to 0.870, according to the accepted criteria from the literature [37].

3.5. Photodynamic properties: singlet oxygen determination

Fig. 4 shows the semilogarithmic plots describing the progress of reaction for DMA in DMF photosensitized by MB, NR and NRBr. The values of the observed rate constant (k_{obs}) were obtained and Φ_Δ was calculated according to eq. (6) (Table 3).

A higher efficiency in the $^1O_2$ production was determined for NRBr, which was about 2.7 fold higher than the lead compound. This could be explained in terms of heavy-atom effect.

A value of $\Phi_\Delta = 1.16$ for NR was determined in experimental conditions at which the λ_{max} of the dye was of 450 nm, while Phoenix et al. reported a value of $\Phi_\Delta = 0.18$ for the same compound at λ_{max} at 536 nm [38]. According to our previous work, the bands at 450 nm and 536 nm correspond to the monomeric and aggregate forms of NR respectively [15]. Taking into account that the values of

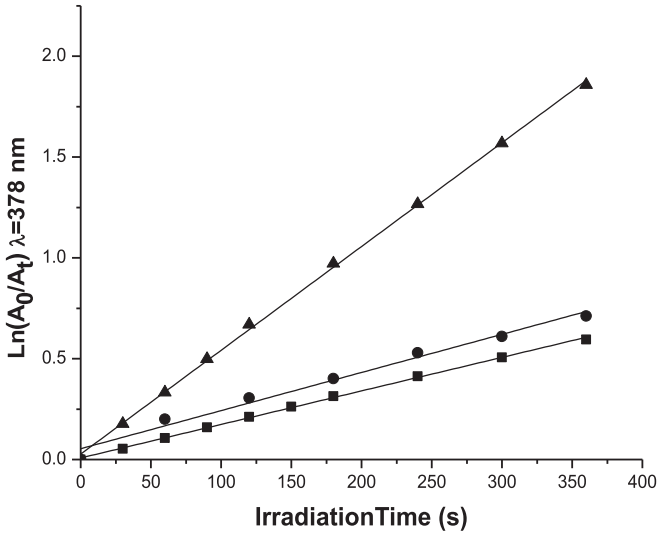

Fig. 4. First-order plots for the photooxidation of DMA photosensitized by MB (■), NR (●) and NRBr (▲) in DMF.

$^1O_2$ can diminish when the PS is partially aggregated [39], the low Φ_Δ value reported earlier for this dye compared to our determination can be explained because under the present experimental conditions, the dye existed only as monomer species; consequently, Φ_Δ was even higher than the reference MB value.

3.6. Antimicrobial PACT

Several parameters were checked in order to assess the PACT of bacterial cells of the newly synthesized monobromo derivative, and the results were compared to that exhibited by NR. Both PS were initially dissolved in a mixture of DMF: aqueous solution (1:9 v/v) and then diluted with PBS, assessing the photoantimicrobial action at different concentrations of the dye. The final concentration of DMF present in such dilutions did not alter cell viability (data not shown).

No significant variation in the number of viable cells was observed in *S. aureus* cultures illuminated for up to 60 min when they were compared with the control groups ($P > 0.05$) (data not shown).

Fig. 5 shows the survival of *S. aureus* ATCC 25923 exposed to a wide range of (A) NRBr and (B) NR concentrations at different irradiation times and incubated in dark. Both PS assayed were not toxic for this species in the dark at a concentration up to 200 μM. This indicates that the death of the cell obtained after irradiation of cultures treated with NRBr or NR is due to the effect of the photosensitizing agents produced by the visible light. The phototoxicity of NRBr toward this bacterium was higher than that of NR (compare Fig. 5A and B), and displayed a dependent effect on both time-exposure and concentration. The viable count for the three exposure times substantially decreased, yielding ≥ 4 $\log_{10}$ reduction in

Table 2
Parameters and statistical data of correlation between log k_w and clog P values.

	a	b	r	s	F
OSIRIS	1.6 ± 0.2	−2.1 ± 0.8	0.913	2.925	74.053
miLogP	1.4 ± 0.2	−1.4 ± 0.8	0.892	3.164	58.775
ACD/logP	1.8 ± 0.3	−2 ± 1	0.870	5.681	47.887

a: slope; b: intercept; r: r-square; s: residual sum of squares; F: value of the Fisher test of significance.

Table 3
Kinetic parameters for the photooxidation of DMA in DMF sensitized by MB, NR and NRBr and singlet oxygen quantum yield (Φ_Δ).

Compound	k_{obs} (s^{-1})	Φ_Δ[a]
Methylene Blue (MB)	$(166 \pm 2) \times 10^{-5}$	1.00
Neutral Red (NR)	$(19 \pm 1) \times 10^{-4}$	1.16
Neutral Red monobrominated (NRBr)	$(515 \pm 5) \times 10^{-5}$	3.14

[a] Relative to Methylene Blue.

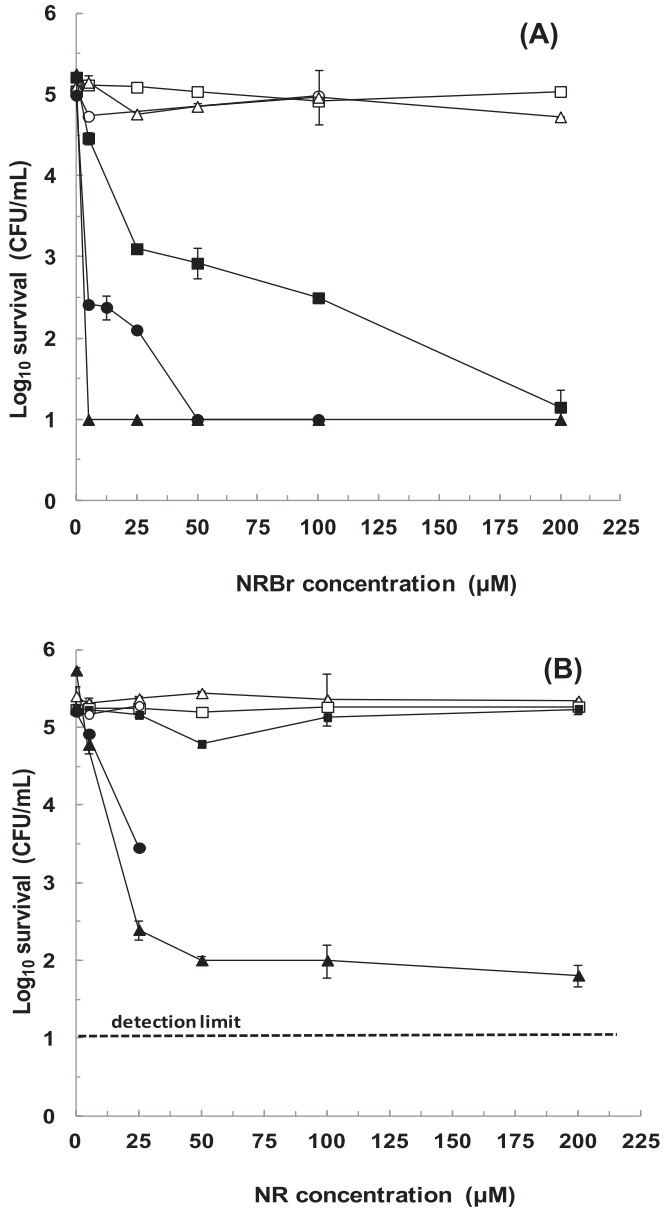

Fig. 5. Photodynamic inactivation of *S. aureus* ATCC 25923 (10^5 CFU/mL) treated with a range of concentrations of NRBr (A) or NR (B) and exposed to visible light for different irradiation times: (■) 15 min, (●) 30 min and (▲) 60 min. Open symbols are controls exposed to the PS without irradiation. Values represent mean ± standard deviation of three separate experiments.

the presence of 50 μM NRBr after 30 min exposure. Under these experimental conditions the detection limit of the method was reached. Furthermore, no viable bacterium was detected after 60 min exposure in the whole range of the NRBr concentrations assayed (5–200 μM). By contrast, none of the tested concentrations of NR was sufficient to produce full photoinactivation of this microorganism (Fig. 5B), even at longer irradiation times (60 min). The greatest effect exhibited by this PS (~3.2 $\log_{10}$ decrease in cell survival) was observed when the culture was treated with 50 μM of sensitizer and irradiated for 60 min; however, there was no significant change in microbial photoinactivation when the concentration of this PS increased. Similar level of viability reduction of this Gram-positive bacterium was obtained when the cultures were exposed to 25 μM NRBr and only to 30 min of irradiation. This demonstrates the superior performance of NRBr derivative for photodynamic inactivation of *S. aureus*.

In view of the performance exhibited by the new NRBr derivative, 30 min of irradiation was selected for the following studies.

The effect of cell density on the PACT was evaluated by comparing 10^5 and 10^7 CFU/mL. This condition was selected according to the guidelines for the determination of susceptibility to antimicrobial agents used in current therapies [40]. Fig. 6 shows that the light-mediated killing of *S. aureus* incubated with NRBr reached ~5 $\log_{10}$ at cell density of 10^7 CFU/mL. At the same time, *S. aureus* showed ≥4 $\log_{10}$ killing which is equivalent to eradication in this experimental conditions when the lowest cell concentration was used.

Therefore, the $\log_{10}$ reduction achieved under both experimental conditions was similar. Since in each experiment different starting inocula were assayed, the detection limit was reached only with the lowest inoculum, while in the other experiment some surviving bacteria were recovered.

In general, previous reports suggest that the effectiveness of the PACT for other PS increases with the decrease in cell density. However, differences attributed to the degree of binding of PS to microbes were observed [41]. In particular, a lack of dependence on cell density was described for Rose Bengal against *S. aureus*. This behavior of Rose Bengal, among others tested, was attributed to the entrance of PS by a diffusion controlled process.

Fig. 7 shows the antibacterial efficacy of NRBr and NR in the clinical isolate MRSA61 under both dark and light conditions. Application of visible light in the absence of PS showed no significant difference compared to the control groups ($P > 0.05$). The viability of this isolate was not affected by dark incubation with both PS for 30 min.

After illumination, NRBr showed a much higher level of killing than NR. NRBr also exhibited a significant concentration-dependent effect until 50 μM (~3.7 $\log_{10}$ killing) against MRSA61. However, the concentration dependence for NR was not observed.

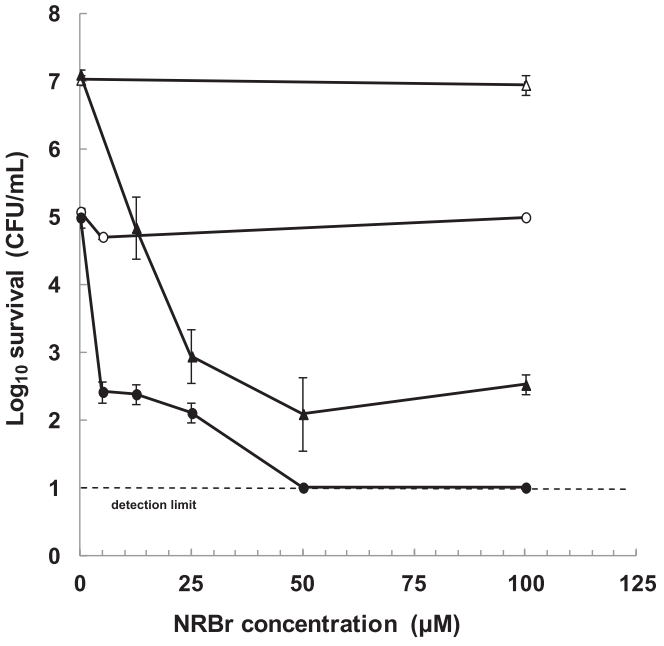

Fig. 6. Photoinactivation of *S. aureus* ATCC 25923 at 10^7 CFU/mL (▲, △) and 10^5 CFU/mL (●, ○). Cells were incubated with the specified concentration of NRBr and illuminated for 30 min. The values are the mean of three independent experiments. Open symbols are cultures maintained in dark.

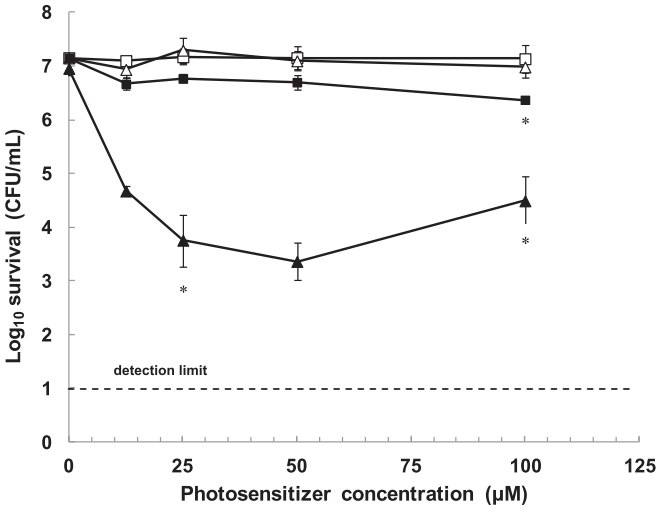

Fig. 7. Photodynamic inactivation of MRSA61 (10^7 CFU/mL) treated with a range of concentrations of photosensitizers. (□) and (△) are controls non-irradiated and exposed to NR and NRBr, respectively. (■) and (▲) are cultures treated with NR and NRBr, respectively, exposed to visible light for 30 min. Values represent mean ± standard deviation of two separate experiments. *, $P < 0.05$, compared with previous concentration assayed.

Only significant differences were observed when 100 μM NR was evaluated.

The performance exhibited by NRBr for PACT of the isolates assayed was compared to sensitive *S. aureus* (Fig. 6) and resistant isolate to current antimicrobial therapeutic use (Fig. 7) under the same conditions of bacterial density, PS concentration and irradiation time. This comparison demonstrated that *S. aureus* ATCC 25923 was more likely to be killed than the clinical MRSA. NRBr at 25 μM and 50 μM led to 4.2 and 5.0 $\log_{10}$ killing, respectively, for *S. aureus* ATCC 25923, while the same concentrations led to 3.3 and 3.7 $\log_{10}$ killing, respectively for MRSA61.

The results available in the literature on PS structurally related to those evaluated in this study do not allow any definitive conclusion when comparing the efficiency of photoinactivation of susceptible and antimicrobial-resistant strains. The performance exhibited by NRBr against methicillin-sensible and -resistant *S. aureus* was similar to that reported by Kashef et al. for Toluidine Blue O [42], while other researchers came up with opposite results [43].

NRBr concentrations greater than 50 μM exhibited reduction of the PACT against both isolates at a bacterial density of 10^7 CFU/mL (Figs. 6 and 7). This behavior was confirmed by other experiments that evaluated the effect of NRBr at concentrations of 50, 100 and 200 μM (data not shown). However, this effect was not observed when an inoculum of 10^5 CFU/mL was evaluated (Fig. 5A).

Our results are in agreement with a previous study on MB and Toluidine Blue O, which showed reduction of the PACT at high concentration of the dyes. This behavior was attributed to an aggregation effect [44]. An additional dimerization of MB and Toluidine Blue O induced by increasing concentrations of bacteria has also been reported [45]. Therefore, the significant reduction of the PACT observed in this work at high NRBr concentrations and 10^7 CFU/mL could be attributed to the aggregation effect.

NR has been used for a long time in different assays for estimation of viable cells in a culture [46,47]. Several reports showed that the brominated derivatives present low to nondeterminable toxicity in different cells [48,49]. In addition, brominated thiazine derivatives exhibit decreased phototoxicity in culture cell compared to the starting reagent [50]. These studies suggest that NR and NRBr would be safe antimicrobial treatments for infections without damaging effects on human cells.

4. Conclusions

Many products can behave as PS and new ones are regularly discovered; however, very few have made it to clinical trial and even fewer are readily commercially available. Each of the currently commercially available PS has specific characteristics, but neither is an ideal agent.

The current work is the first report on initial antimicrobial testing of the new NRBr azine dye and gives an insight into the PACT properties of NR.

The improved photoproperties exhibited by NRBr were accompanied by significant increases in the photoantimicrobial action, showing significant improvements compared to NR. This increase was observed in both isolates, sensitive and resistant to conventional antimicrobial agents. In addition, the improved lipophilicity of NRBr could be another factor that contributes to the observed performance. Thus, it is possible that NRBr concentration in bacteria is significantly higher than that of NR and enough to kill organisms after light irradiation. Additional studies will be needed to confirm this hypothesis.

Furthermore, although both PS showed aggregation under the conditions evaluated, the bacterial photoinactivation exhibited by the monobrominated derivative was affected to a lesser extent than that of NR.

Although PACT against MRSA clinical isolate was slightly lower than that observed for the collection strain sensitive to antimicrobials, more isolates should be evaluated to reach definitive conclusions in this regard.

In conclusion, the new compound NRBr showed striking properties, which are important outcomes for PDT and PACT. It also exhibited higher *in vitro* photoantimicrobial effect against *S. aureus* than the starting reagent. These preliminary results suggest that the new compound could be a promising PS to be used in photodynamic therapeutic applications.

Acknowledgments

We are grateful for the financial support of this research from Secretaría de Ciencia y Técnica de la Universidad Nacional de Córdoba (SECYT-UNC, Nº 162/12) and Fondo para la Investigación Científica y Tecnológica (FONCYT, Nº 109/08) of Argentina.

The authors wish to express their sincere thanks to Dr. Ruben H. Manzo for allowing us to use the Evolution 300 spectrophotometer. We also thank Dra. Veronica Romero and Lic. Qca. Farm. Clarisa Rosset for technical support. F.L.A. is a scientific Member of CONICET. M.N.U. thanks CONICET for its research fellowships.

Appendix A. Supplementary data

Supplementary data related to this article can be found at http://dx.doi.org/10.1016/j.dyepig.2014.12.021.

References

[1] Master A, Livingston M, Sen Gupta A. Photodynamic nanomedicine in the treatment of solid tumors: perspectives and challenges. J Control Release 2013;168(1):88–102.
[2] Alves E, Faustino MA, Tomé JP, Neves MG, Tomé AC, Cavaleiro JA, et al. Nucleic acid changes during photodynamic inactivation of bacteria by cationic porphyrins. Bioorg Med Chem 2013;21(14):4311–8.
[3] Robertson CA, Evans DH, Abrahamse H. Photodynamic therapy (PDT): a short review on cellular mechanisms and cancer research applications for PDT. J Photochem Photobiol B 2009;96(1):1–8.

[4] Milanesio ME, Spesia MB, Cormick MP, Durantini EN. Mechanistic studies on the photodynamic effect induced by a dicationic fullerene C60 derivative on *Escherichia coli* and *Candida albicans* cells. Photodiagnosis Photodyn Ther 2013;10(3):320–7.
[5] Hanakova A, Bogdanova K, Tomankova K, Pizova K, Malohlava J, Binder S, et al. The application of antimicrobial photodynamic therapy on *S. aureus* and *E. coli* using porphyrin photosensitizers bound to cyclodextrin. Microbiol Res 2014;169(2–3):163–70.
[6] Nishiyama N, Morimoto Y, Jang WD, Kataoka K. Design and development of dendrimer photosensitizer-incorporated polymeric micelles for enhanced photodynamic therapy. Adv Drug Deliv Rev 2009;61(4):327–38.
[7] Rossetti FC, Lopez LB, Carollo AR, Thomazini JA, Tedesco AC, Bentley MV. A delivery system to avoid self-aggregation and to improve in vitro and in vivo skin delivery of a phthalocyanine derivative used in the photodynamic therapy. J Control Release 2011;155(3):400–8.
[8] Paszko E, Ehrhardt C, Senge MO, Kelleher DP, Reynolds JV. Nanodrug applications in photodynamic therapy. Photodiagn Photodyn Ther 2011;8:14–29.
[9] Singh MK, Pal H, Bhasikuttan AC, Sapre AV. Dual solvatochromism of Neutral Red. Photochem. Photobiol 1998;68(1):32–8.
[10] Sousa C, Sá e Melo T, Gèze M, Gaullier JM, Mazière JC, Santus R. Solvent polarity and pH effects on the spectroscopic properties of neutral red: application to lysosomal microenvironment probing in living cells. Photochem Photobiol 1996;63(5):601–7.
[11] Basu S, Panigrahi S, Praharaj S, Ghosh SK, Pande S, Jana S, et al. Solvent effect on the electronic spectra of azine dyes under alkaline condition. J Phys Chem A 2007;111(4):578–83.
[12] Fischer BB, Krieger-Liszkay A, Eggen RIL. Oxidative stress induced by the photosensitizers neutral red (type I) or rose bengal (type II) in the light causes different molecular responses in *Chlamydomonas reinhardtii*. Plant Sci 2005;168(3):747–59.
[13] Yen GSL, Simon EH. Photosensitization of herpes simplex virus type 1 with Neutral Red. J Gen Virol 1978;41:273–81.
[14] Phoenix DA, Sayed Z, Hussain S, Harris F, Wainwright M. The phototoxicity of phenothiazinium derivatives against *Escherichia coli* and *Staphylococcus aureus*. FEMS Immunol Med Microbiol 2003;39(1):17–22.
[15] Urrutia MN, Ortiz CS. Spectroscopic characterization and aggregation of azine compounds in different media. Chem Phys 2013;142(1):41–50.
[16] Shao W, Wang H, He S, Shi L, Peng K, Lin Y, et al. Photophysical properties and singlet oxygen generation of three sets of halogenated corroles. J Phys Chem B 2012;116(49):14228–34.
[17] Lin CW, Shulok JR, Wong YK, Schanbacher CF, Cincotta L, Foley JW. Photosensitization, uptake, and retention of phenoxazine nile blue derivatives in human bladder carcinoma cells. Cancer Res 1991;51(4):1109–16.
[18] Dutta P, Rai R, Pandey S. Effect of ionic liquid on J-aggregation of meso-tetrakis(4-sulfonatophenyl)porphyrin within aqueous mixtures of poly(ethylene glycol). J Phys Chem B 2011;115(13):3578–87.
[19] Choudhury SD, Bhasikuttan AC, Pal H, Mohanty J. Surfactant-induced aggregation patterns of thiazole orange: a photophysical study. Langmuir 2011;27(20):12312–21.
[20] Wiczling P, Struck-Lewicka W, Kubik L, Siluk D, Markuszewski MJ, Kaliszan R. The simultaneous determination of hydrophobicity and dissociation constant by liquid chromatography-mass spectrometry. J Pharm Biomed Anal 2014;94:180–7.
[21] Desroches MC, Layac S, Prognon P, Maillard P, Grierson DS, Curis E, et al. Speciation of new tri- and tetra-glucoconjugated tetrapyrrolic macrocycles (porphyrins and chlorins): an electronic molecular spectroscopy study. Appl Spectrosc 2003;57(8):950–9.
[22] Gualdesi MS, Ravetti S, Raviolo MA, Briñón MC. Preformulation studies of novel 5′-O-carbonates of lamivudine with biological activity: solubility and stability assays. Drug Dev Ind Pharm 2013:1–7.
[23] Piechocki JT, editor. Pharmaceutical photostability and stabilization technology. Drugs and pharmaceutical sciences. New York: Thoma Karl; 2010.
[24] Pallicer JM, Pous-Torres S, Sales J, Rosés M, Rafols C, Bosch E. Determination of the hydrophobicity of organic compounds measured as log Po/w through a new chromatographic method. J Chromatogr A 2010;1217(18):3026–37.
[25] Pitucha M, Polak B, Swatko-Ossor M, Popiołek Ł, Ginalskac G. Determination of the lipophilicity of some new derivatives of thiosemicarbazide and 1,2,4-triazoline-5-thione with potential antituberculosis activity. Croat Chem Acta 2010;83(3):299–306.
[26] Rolim JP, de-Melo MA, Guedes SF, Albuquerque-Filho FB, de Souza JR, Nogueira NA, et al. The antimicrobial activity of photodynamic therapy against Streptococcus mutans using different photosensitizers. J Photochem Photobiol B 2012;106:40–6.
[27] Cincotta L, Foley JW, Cincotta AH. Novel red absorbing benzo[a]phenoxazinium and benzo[a]phenothiazinium photosensitizers: in vitro evaluation. Photochem Photobiol 1987;46(5):751–8.
[28] Ravetti S, Gualdesi MS, Briñón MC. Lipophilicity of 5′-carbonates of lamivudine with antiretroviral activity. Correlation between different methods. J Liq Chromatogr Relat Technol 2008;31:1014–32.
[29] Griffin S, Grant Wyllie S, Markham J. Determination of octanol-water partition coefficient for terpenoids using reversed-phase high-performance liquid chromatography. J Chromatogr A 1999;864(2):221–8.
[30] Casoni D, Cobzac CS, Sarbu C. A comparative study concerning the lipophilicity of some synthetic dyes estimated by thin layer chromatography and different computation methods. Rev Chim 2010;61(3):229–34.
[31] Singh MK, Pal H, Bhasikuttan AC, Sapre AV. Photophysical properties of the cationic form of neutral red. Photochem Photobiol 1999;69(5):529–35.
[32] Goicoechea J, Arregui FJ, Corres JM, Matias IR. Study and optimization of self-assembled polymeric multilayer structures with Neutral Red for pH sensing applications. J Sensors 2008:1–7.
[33] Chen SM, Lin KC. The electrocatalytic properties of polymerized neutral red film modified electrodes. J Electroanal Chem 2001;511:101–14.
[34] Ghasemi J, Niazi A, Kubista M. Thermodynamics study of the dimerization equilibria of rhodamine B and 6G in different ionic strengths by photometric titration and chemometrics method. Spectrochim Acta Part A 2005;62:649–56.
[35] Sztanke K, Markowski W, Swieboda R, Polak B. Lipophilicity of novel antitumor and analgesic active 8-aryl-2,6,7,8-tetrahydroimidazol[2,1-c][1,2,4]triazine-3,4-dione derivatives determined by reversed-phase RP-HPLC and computational methods. Eur J Med Chem 2010;45:2644–9.
[36] Friberg EG, Cunderlíková B, Pettersen EO, Moan J. pH effects on the cellular uptake of four photosensitizing drugs evaluated for use in photodynamic therapy of cancer. Cancer Lett 2003;195(1):73–80.
[37] Mrkvičková Z, Kovaříková P, Balíková S, Klimeš J. Determination of lipophilicity of novel potential antituberculotic agents using HPLC on monolithic stationary phase and theoretical calculations. J Pharm Biomed Anal 2008;48:310–4.
[38] Phoenix DA, Harris F. Phenothiazinium-based photosensitizers: antibacterials of the future? TRENDS Mol Med 2003;9(7):283–5.
[39] Lim CK, Heo J, Shin S, Jeong K, Seo YH, Jang WD, et al. Nanophotosensitizers toward advanced photodynamic therapy of cancer. Cancer Lett 2013;334(2):176–87.
[40] Clinical and Laboratory Standards Institute. Methods for dilution antimicrobial susceptibility tests for bacteria that grow aerobically. 7° ed. Wayne, PA: CLSI Publication M7-A7; 2006. approved standard.
[41] Demidova TN, Hamblin MR. Effect of cell-photosensitizer binding and cell density on microbial photoinactivation. Antimicrob Agents Chemother 2005;49(6):2329–35.
[42] Kashef N, Abadi GRS, Djavid GE. Phototoxicity of phenothiazinium dyes against methicillin-resistant *Staphylococcus aureus* and multi-drug resistant *Escherichia coli*. Photodiagnosis Photodyn Ther 2012;9:11–5.
[43] Tang HM, Hamblin MR, Yow CMN. A comparative in vitro photoinactivation study of clinical isolates of multidrug-resistant pathogens. J Infect Chemother 2007;13(2):87–91.
[44] Goinho Vilela SF, Campos Junqueira J, Oliveira Barbosa J, Majewski M, Munin E, Cardoso Jorge AO. Photodynamic inactivation of *Staphylococcus aureus* and *Escherichia coli* biofilms by malachite green and phenothiazine dyes: an in vitro study. Arch Oral Biol 2012;57:704–10.
[45] Usacheva MN, Teichert MC, Biel MA. The role of methylene blue and toluidine blue monomers and dimers in the protoinactivation of bacteria. J Photochem Photobiol B 2003;71:87–98.
[46] Gray DWR, Millard PR, McShane P, Morris PJ. The use of the dye neutral red as a specific, non-toxic, intra-vital stain of islets of langerhans. Br J Exp Path 1983;64:553–8.
[47] Repetto G, del Peso A, Zurita JL. Neutral red uptake assay for the estimation of cell viability/cytotoxicity. Nat Protoc 2008;3(7):1125–31.
[48] Gorman A, Killoran J, O'Shea C, Kenna T, Gallagher WM, O'Shea DF. In vitro demonstration of the heavy-atom effect for photodynamic therapy. J Am Chem Soc 2004;126:10619–31.
[49] Lacerda SHD, Abraham B, Stringfellow TC, Indig GL. Photophysical, photochemical, and tumor-selectivity properties of bromine derivatives of Rhodamine-123. Photochem Photobiol 2005;81:1430–8.
[50] Montes de Oca MN, Vara J, Milla L, Rivarola V, Ortiz CS. Physicochemical properties and photodynamic activity of novel derivatives of triarylmethane and thiazine. Arch Pharm Chem Life Sci 2013;346:255–65.